Title
Analysis of Nanofluid-Based Parabolic Trough Collectors for Solar Thermal Applications

Journal
Journal of Solar Energy Engineering, 140(5)

ISSN
0199-6231

Authors
Freedman, Justin P
Wang, Hao
Prasher, Ravi S

Publication Date
2018-10-01

DOI
10.1115/1.4039988

Peer reviewed

Analysis of Nanofluid-Based Parabolic Trough Collectors for Solar Thermal Applications

Justin P. Freedman[1], Hao Wang[1], Ravi S. Prasher[1,2,*]

[1]Energy Storage and Distributed Resources Division, Lawrence Berkeley National Laboratory, 1 Cyclotron Road, Berkeley, CA 94720

[2]Department of Mechanical Engineering, University of California, Berkeley, CA 94720

*Corresponding author: rsprasher@lbl.gov

Keywords: Nanofluid; volumetric absorption; concentrated solar power (CSP); parabolic trough collector (PTC)

Solar-to-thermal energy conversion technologies are an important and increasingly promising segment of our renewable energy technology future. Today, concentrated solar power plants provide a method to efficiently store and distribute solar energy. Current industrial solar-to-thermal energy technologies employ selective solar absorber coatings to collect solar radiation, which suffer from low solar-to-thermal efficiencies at high temperatures due to increased thermal emission from selective absorbers. Solar absorbing nanofluids (a heat transfer fluid seeded with nanoparticles), which can be volumetrically heated, are one method to improve solar-to-thermal energy conversion at high temperatures. To date, radiative analyses of nanofluids via the radiative transfer equation have been conducted for low temperature applications and for flow conditions and geometries that are not representative of the technologies used in the field. In this work, we present the first comprehensive analysis of nanofluids for concentrated solar power plants in a parabolic trough configuration. This geometry was chosen because parabolic troughs are the most prevelant CSP technologies. We demonstrate that the solar-to-thermal energy conversion efficiency can be optimized by tuning the nanoparticle volume fraction, the temperature of the nanofluid, and the incident solar concentration. Moreover, we demonstrate that direct solar absorption

receivers have a unique advantage over current surface-based solar coatings at large tube diameters. This is because of a nanofluid's tunability, which allows for high solar-to-thermal efficiencies across all tube diameters enabling small pressure drops to pump the heat transfer fluid at large tube diameters.

Nomenclature

Ag = Silver
c = Specific heat capacity
C_p = Volumetric heat capacity
CSP = Concentrated solar power
$C_1 = 1.8706 \times 10^{-16}$ W m^2
$C_2 = 0.014388$ m K
f_v = Volume fraction of Ag nanoparticles seeded in Therminol VP-1
HTF = Heat transfer fluid
$I_{bb,\lambda}$ = Spectral blackbody intensity per unit steradian
J_λ = Spectral intensity per unit angle
k = Thermal conductivity
k_{Ag} = Imaginary part of the refractive index of silver
$k_{Therminol}$ = Imaginary part of the refractive index of Therminol VP-1
L_x = Length of the tube in the x-direction
L_y = Length of the tube in the y-direction
L_z = Length of the tube in the z-direction
$\dot{m}$ = Mass flow rate
n_{Ag} = Real part of the refractive index of silver
$n_{Therminol}$ = Real part of the refractive index of Therminol VP-1
n_{Vacuum} = Real part of the refractive index of a vacuum
PTC = Parabolic trough collector
T = Temperature
T_{in} = Inlet temperature of the heat transfer fluid
T_{out} = Outlet temperature of the heat transfer fluid
T_{sun} = Blackbody temperature of the sun
q_{inc} = Incident heat flux
q_r = Radiative heat flux
$q_{r,\lambda}$ = Spectral radiative heat flux
u = Velocity of the fluid
x = Position in the x-direction
y = Position in the y-direction
η = Solar-to-thermal efficiency
$\theta_{critical}$ = Critical angle based on Snell's law
λ = Wavelength
μ = Directional cosine

ρ_0 = Reflectivity of the $y = 0$ surface
ρ_L = Reflectivity of the $y = L_y$ surface
$\rho_{Therminal}$ = Viscosity of Therminl VP-1
σ = the radiative absorption coefficient
σ_{Stefan} = Stefan-Boltzmann constant
τ = Optical thickness

1. Introduction

Solar-to-thermal energy conversion plays an important role in many renewable energy technologies, such as concentrated solar power (CSP) electricity production, water heating, thermochemical reactions, and thermal energy-based water desalination. Currently, solar heating of the heat transfer fluid (HTF) in most applications is achieved by first heating a surface that is coated with a selective solar absorber. Selective solar absorbers exhibit high optical absorptivity in the solar spectrum while suppressing thermal re-emission in the infrared spectrum. The heated surface then transfers the thermal energy via convection to the underlying HTF. The main drawbacks of surface-based heating are the low solar-to-thermal efficiencies, η, at high temperatures [1] and the instability of the selective solar absorber coatings at high temperatures (> 800 K) [2]. One method to increase η in these systems is to seed the HTF with absorbing nanoparticles, producing a fluid known as a nanofluid [3-5]. The seeding of HTFs with nanoparticles is a concept that originally dates back as far as the 1970s [6-8].

Nanoparticle seeding is an approach that allows for direct volumetric absorption of solar radiation into the HTF by making the HTF "black" in the solar spectrum. The advantages of volumetric absorption over selective solar absorbing surfaces are that (1) the temperature differences between the absorbing nanoparticles and the HTF are negligible, (2) volumetric absorption can potentially lead to lower emissive losses at high operating temperatures, and (3)

volumetric receivers allow for simpler designs that reduce the parasitic losses associated with the pressure drop in the receiver tubes.

To date, the research conducted on the use of nanofluids for solar-to-thermal applications can be broadly divided into three categories:

1) Low temperature applications: Nanofluids have been evaluated in flat plate collectors for low temperature applications [3, 4, 9]. In these articles the radiation analysis was greatly simplified by neglecting the thermal re-emission term in the equation of radiative transport. Neglecting thermal re-emission is a poor approximation for high temperature applications.
2) High temperature falling films: Tien and coworkers [10, 11] provided a thorough framework for investigating the radiative transfer equation in a falling film geometry. Here, the HTF's inlet temperature was 561 K and the flow was assumed to be laminar. The falling film receiver is not a widely used geometry and in the majority of parabolic trough receivers the flow is turbulent, rather than laminar. These papers also did not investigate if there was an optimal volume fraction of the nanoparticles in the nanofluid for which η could be maximized.
3) High temperature stagnant fluid: This research was conducted by Lenert and Wang [1]. While this work provided a preliminary analysis that identified a single optimized optical depth, it was conducted for a stagnant fluid, which is not reflective of real world systems where the fluid is flowing.

In this paper, we have removed the assumptions from the previous studies listed above to provide the first comprehensive analysis of η optimization in volumetric receivers. We demonstrate that η is dependent upon the HTF's inlet temperature, the incident solar concentration,

and the nanofluid materials. We conducted our study based on inlet temperatures and concentration factors used in real-world parabolic trough CSP plants. The parabolic trough configuration for concentrated solar power generation is one of the most widely used solar collector geometries for applications ranging from concentrated solar power plants to industrial process heating [12]. However, no radiative transfer analysis has been conducted on the use of nanofluids in a parabolic trough configuration. The salient features of our analysis are (1) the incorporation of thermal re-emission in the RTE, (2) the use of a turbulent flow model instead of laminar flow, which is the case in parabolic trough CSP plants, (3) a realistic quasi-two-dimensional geometry that accurately models a parabolic trough configuration, (4) a comprehensive analysis of η optimization, (5) the use of a Therminol-based nanofluid (Therminol is a widely used HTF in parabolic trough collectors), and (6) the effects of receiver tube dimensions on η and pressure drop.

The main findings of the paper are (1) that there is an optimal volume fraction/optical depth for which η is maximized, (2) the value of η is independent of tube diameter in the low nanoparticle volume fraction regime, and (3) the value of η in volumetric receivers is far less sensitive to receiver dimensions than in surface-based receivers. This conclusion has significant implications for the pressure drop in solar-to-thermal systems and their associated parasitic power losses.

2. Numerical Model

2.1 Geometry of the receiver

A schematic of the direct solar volumetric absorption receiver is shown in Figure 1. Parabolic trough collectors (PTCs) use circular tubes with an inner diameter that are 10s of millimeters in length. To accurately model volumetric absorption of the solar spectrum and thermal re-emission in the infrared spectrum the RTE must be solved. Solving the RTE in a cylindrical

geometry adds significant and unnecessary complexity. Therefore, we instead modeled a square tube in Cartesian coordinates to enable a full solution of the RTE ($L_y = L_z$). This approximation is demonstrated in Figure 1, where the real-world circular geometry is shown on the left and the approximated rectangular geometry used in this study is shown on the right. A square tube is a reasonable approximation because the length of the receiver tube is much greater than the hydraulic diameter of the tube. For example, SkyFuel Inc.'s© (a manufacturer of PTCs) Sky Trough® PTC is 115 m in length compared to a tube diameter of 76 mm for the Schott PTR 80^{TM} linear receiver. In most CSP plants 8 to 10 PTCs are combined in series for a total x-axis length of 920 m. Based on these two industrial products we have chosen to use values of $L_x = 920$ m and a nominal value of $L_y = 76$ mm in our analysis.

The HTF in Figure 1 flows in the x-direction with a mass flow rate ($\dot{m}$) of 12 kg/s and the HTF used in this study is Therminol VP-1, a common industrial HTF, seeded with silver (Ag) nanoparticles. A mass flow rate of 12 kg/s is a common flow rate for CSP plants operating at peak conditions [13]. The combination of Therminol VP-1 and Ag nanoparticles was identified by Taylor and coworkers [5] to be a promising solar nanofluid, based on its measured optical properties. The real part of the index of refraction ($n_{\text{Therminol}}$) for Therminol VP-1 is assumed to be 1.65 across the entire spectrum and the imaginary part of Therminol VP-1's index of refraction ($k_{\text{Therminol}}$) is assumed to be 0 [14].

The inlet temperature (T_{in}) of the HTF at $x = 0$ is uniform in the y and z-directions (origin axes are indicated with green arrows on the right side in Figure 1) and the tube is thermally insulated within a vacuum. This is analogous to industrial PTC receiver tubes, where the HTF is enclosed within a metal (commonly aluminum) tube that is encased within a larger glass tube. The volume between the glass and aluminum tubes is under vacuum to maintain high HTF temperatures with no

convective thermal losses. The sketch on the left side of Figure 1 shows the two concentric tubes surrounding the HTF. To simplify the analysis in our study, we assume that the two concentric tubes are made of a material that is optically transparent across the solar and infrared spectrums and has a refractive index, $n_{\text{Tube}} = 1$. However, this assumption does not affect any of the conclusions because incorporating the refractive index of the enclosing tube will only change the critical angle and reflectivity at the surface. This can be easily incorporated in a more detailed model. In a real system the reflection at the outer surface of both the outer tube and the inner tube can be reduced by using an anti-reflection coating.

The incident solar radiation is concentrated by a parabolic trough collector and creates a two-dimensional semi-circle upon which the incident solar radiation is distributed on one of the receiver's surfaces. Although the incident solar radiation is not evenly distributed in industrial PTCs [15, 16], we have approximated the distribution to be evenly distributed over the two-dimensional semi-circle to simplify our analysis. A more detailed model can incorporate the actual distribution of solar flux. The difference in the vacuum and HTF's index of refraction causes the incident semi-circular radiation to be further concentrated inside the HTF, as shown in Figure 1, where the angle between the y-axis and the cone of incident radiation is equal to the critical angle, based on Snell's Law. The top side of the receiver, $y = 0$, is surrounded by vacuum with an index of refraction equal to one, $n_{\text{Vacuum}} = 1$, and the inner wall at the bottom of the receiver, $y = L_y$, has a gray reflectivity equal to one, where $\rho_L = 1$. A gray reflectivity of $\rho_L = 1$ at the bottom of the receiver simplifies the solution and is a reasonable approximation that does not influence the results of the model because most of the light is absorbed before striking the bottom surface.

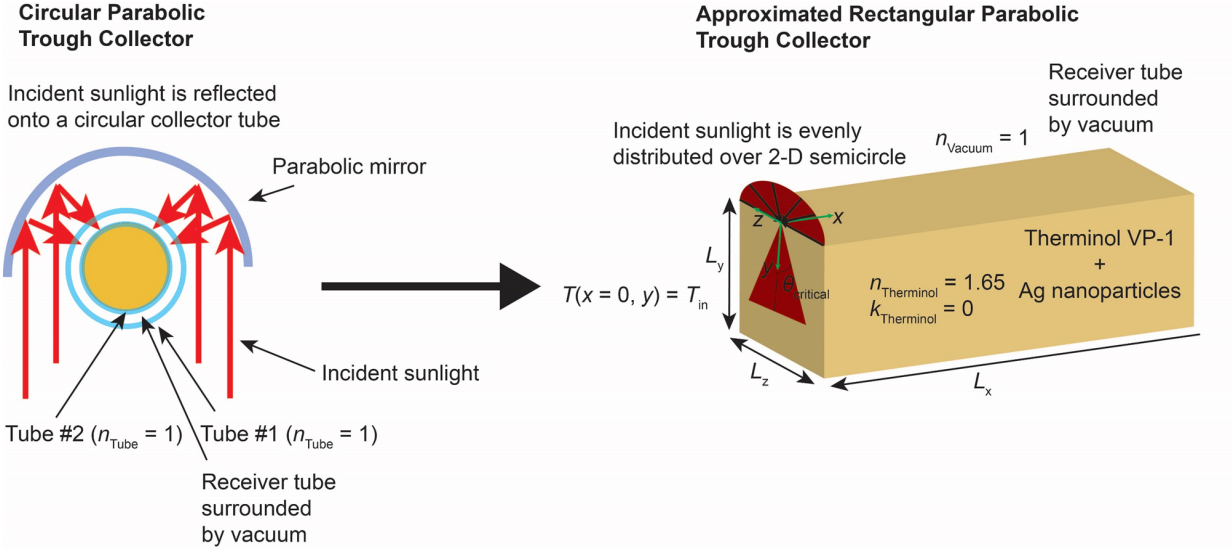

Figure 1: On the left is a depiction of the real-world circular geometry of a parabolic trough collector and on the right is the approximated rectangular geometry used in this study to solve the RTE. For simplicity, we have assumed that the liquid is surrounded by a material with refractive index of, n_{Tube} = 1 (the same as vacuum). This does not affect any conclusions of the paper as the refractive index of the surrounding/enclosing medium only affects the critical angle and the reflectivity at the surface, which can be easily incorporated into a detailed model. On the sketch on the right side of the sketch, the incident solar radiation enters the fluid in a cone of concentrated sunlight with an angle between the cone and the tube equal to the critical angle based on Snell's law. The HTF is Therminol VP-1 seeded with Ag nanoparticles and the inlet temperature is uniform across the *y*-axis. The reflectivity of the bottom of the receiver is gray, where ρ_L = 1. The receiver is encased in a vacuum that eliminates thermal convection losses.

2.2 Solution methodology

Accurately modeling solar volumetric absorption within a nanofluid-based HTF and thermal re-emission in the infrared spectrum requires that the radiative intensity fields in the RTE be numerically determined on a directional and spectral basis. To do this, radiative transfer was locally modeled as a quasi-one-dimensional system and the resulting heat flux was used to iteratively determine the subsequent *x*-position's temperature profile in the *y*-direction. This is a valid assumption because the tube diameter (76 mm) is much less than the length of the collector tube (920 m) causing the radiative intensity gradients to be steeper across the HTF's *y*-axis than it's *x*-axis. The diameter of the Ag nanoparticles in this study were assumed to be much smaller than the wavelengths of light associated with solar radiation which means that the scattering is in the Rayleigh regime. Therefore, the radiative transfer within the film could be modeled by the following equation [10],

$$\mu \frac{\partial J_\lambda \left(x,y,\mu\right)}{\partial y} = \sigma_\lambda I_{bb,\lambda}\left(T\left(x,y\right)\right) - \sigma_\lambda J_\lambda \left(x,y,\mu\right), \tag{1}$$

where $\mu = \cos\theta$ is the directional cosine measured from the *y*-axis (shown in Figure 1), J_λ is the spectral intensity per unit angle, λ is wavelength, $I_{bb,\lambda}$ is the spectral blackbody intensity per unit steradian, T is temperature, σ is the radiative absorption coefficient, and the scattering term is neglected due to absorption and extinction dominating. The spectral blackbody intensity is defined as

$$I_{bb,\lambda}\left(T\right) = \frac{n_{Therminol}^3 C_1}{\lambda^5\left(e^{C_2/\lambda T}-1\right)}, \tag{2}$$

where λ is the wavelength of light in vacuum and not in the medium, $C_1 = 1.8706 \times 10^{-16}$ W m^2, and $C_2 = 0.014388$ m K. The spectral radiative absorption coefficient can be determined through the following relation, $\sigma = \mathrm{Im}\left[\frac{m_{Ag}^2 - 1}{m_{Ag}^2 + 2}\right]\frac{6\pi n_{Therminol} f_v}{\lambda}$, where f_v is the nanoparticle volume fraction and $m_{Ag} = \frac{n_{Ag} + ik_{Ag}}{n_{Therminol}}$ is the normalized complex index of refraction of Ag. Here, n_{Ag} and k_{Ag} are the real and imaginary components of Ag's refractive index [17, 18]. Figure 2(a) shows the spectral dependence of n_{Ag} and k_{Ag} along with $n_{Therminol}$ while Figure 2(b) shows the spectral dependence on the radiative absorption coefficient for monodispersed Ag nanoparticles seeded in Therminol VP-1 under Rayleigh scattering conditions, where $f_v = 1 \times 10^{-9}$ [19, 20].

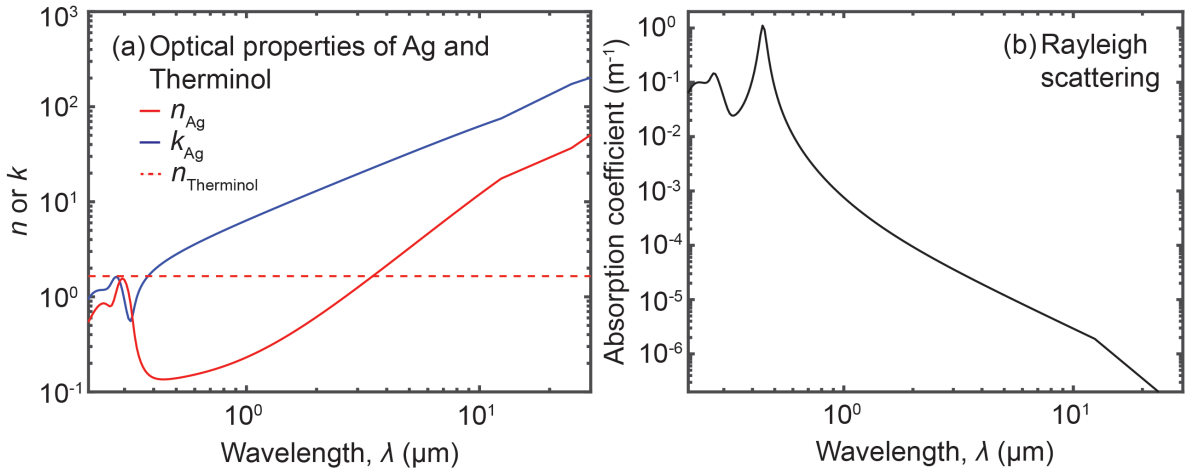

Figure 2: (a) Spectral refractive index of Ag and Therminol VP-1. (b) Spectral radiative absorption coefficient for Ag nanoparticles seeded in Therminol VP-1 under Rayleigh scattering conditions, where $f_v = 1 \times 10^{-9}$.

The spectral and directional intensity at the $y = 0$ boundary is the sum of the incident solar intensity, the radiative intensity from the ambient environment, and the reflected radiative intensity

moving in the negative y-direction at the $y = 0$ boundary. At the $y = L_y$ boundary the spectral and directional intensity is equal to the reflected intensity of radiation moving in the positive y-direction at the boundary. Assuming only specular reflection occurs at both boundaries, the boundary conditions can be expressed as [10]

$$J_\lambda\left(x, y=0, +\mu\right) = A\left(1-\rho_0\left(+\mu\right)\right) I_{bb,\lambda}\left(T_{sun}\right) + \frac{1}{\sin\left(\theta_{critical}\right)}\left(1-\rho_0\left(+\mu\right)\right) I_{bb,\lambda}\left(T_{amb}\right) + \rho_0\left(-\mu\right) J_\lambda\left(x, y=0, -\mu\right), \quad (3)$$

$$J_\lambda\left(x, y=L_y, -\mu\right) = \rho_L\left(+\mu\right) J_\lambda\left(x, y=L_y, +\mu\right), \quad (4)$$

where $+\mu$ and $-\mu$ denote radiation traveling with a positive y-axis component and a negative y-axis component, respectively, ρ_0 is the direction-dependent reflectivity at the vacuum-Therminol VP-1 interface, ρ_L is the direction-dependent reflectivity at $y = L_y$, T_{sun} is the radiative temperature of the sun (5780 K), T_{amb} is the ambient temperature of the environment (300 K), and $A = \frac{q_{inc}}{\sigma_{Stefan} T_{sun}^4 \sin\left(\theta_{critical}\right)}$ is a nanofluid-dependent constant, where q_{inc} is the incident concentrated solar flux and σ_{Stefan} is the Stefan-Boltzmann constant. The constant, A, consists of two components; (1) the solar constant, $\frac{q_{inc}}{\sigma_{Stefan} T_{sun}^4}$, and (2) a geometric factor that accounts for the fact that the incident solar radiation and ambient radiation are evenly distributed over an entire semi-circle when travelling through the vacuum, but are squeezed into a two-dimensional cone within the HTF. This geometric factor can be determined through a conservation of energy analysis within the differential cone angle $d\theta_{Vacuum}$, where $J_{Therminol}\left(x, y=0, +\mu\right)\cos\left(\theta_{Therimnol}\right) d\theta_{Therimnol} = \left(1-\rho_0\left(+\mu\right)\right) J_{Vacuum}\left(x, y=0, +\mu\right)\cos\left(\theta_{Vacuum}\right) d\theta_{Vacuum}$. After

differentiating this equation and using Snell's law, $\frac{n_{Therminol}}{n_{Vacuum}} = \frac{\sin\left(\theta_{Therminol}\right)}{\sin\left(\theta_{Vacuum}\right)}$, the intensity in the HTF as a function of the intensity in the vacuum is found to be equal to $J_{Therminol}\left(x, y=0, +\mu\right) = \frac{1}{\sin\left(\theta_{critical}\right)}\left(1-\rho_0\left(+\mu\right)\right) J_{Vacuum}\left(x, y=0, +\mu\right)$, where $\theta_{critical} = \sin^{-1}\left(\frac{n_{Vacuum}}{n_{Therminol}}\right)$.

Equation 3 assumes that the spectral solar flux is equivalent to a Blackbody at 5780 K and that the heat flux due to the ambient environment acts like a Blackbody at 300 K.

In this analysis, the direction-dependent reflectivity at the $y = 0$ boundary was determined based on Snell's Law

$$\rho_0\left(+\mu\right) = \begin{cases} \left(\frac{1-n_{Therminol}}{1+n_{Therminol}}\right)^2, \mu = 0 \\ \frac{1}{2}\frac{\sin^2\left(\theta_0-\theta\right)}{\sin^2\left(\theta_0+\theta\right)}\left(1+\frac{\cos^2\left(\theta_0+\theta\right)}{\cos^2\left(\theta_0-\theta\right)}\right), 0<\mu\le 1 \end{cases} \tag{5}$$

$$\rho_0\left(-\mu\right) = \begin{cases} \left(\frac{1-n_{Therminol}}{1+n_{Therminol}}\right)^2, \mu = 0 \\ \frac{1}{2}\frac{\sin^2\left(\theta-\theta_0\right)}{\sin^2\left(\theta+\theta_0\right)}\left(1+\frac{\cos^2\left(\theta+\theta_0\right)}{\cos^2\left(\theta-\theta_0\right)}\right), 0<\mu\le 1 \end{cases} \tag{6}$$

$$\rho_L\left(+\mu\right) = 1 \tag{7}$$

where $\theta = \cos^{-1}(\mu)$ is the polar angle at which the radiation travels through the Therminol VP-1 with respect to the *y*-axis and $\theta_0 = \sin^{-1}\left(\frac{n_{Therminol}\sin(\theta)}{n_{Vacuum}}\right)$ is the polar angle at which the radiation travels with respect to the *y*-axis on the vacuum side of the boundary. Note that in Equations 5 and 6 it is assumed that the refractive index of the nanofluid is same as Therminol, which is a good assumption as long as the volume fraction of the nanoparticles is very small. In this paper the volume fraction is lower than 0.001. After determining the spectral and directional radiative intensities, the spectral radiative heat flux, $q_{r,\lambda}$, and total radiative heat flux, q_r, can be computed using the following equations

$$q_{r,\lambda}(x,y) = \int_0^{\pi} J_{\lambda}(x,y)\cos\theta d\theta\,, \tag{8}$$

$$q_r(x,y) = \int_{\lambda} q_{r,\lambda}(x,y)d\lambda\,. \tag{9}$$

After determining the radiative heat flux through the HTF, The temperature rise in the nanofluid-based HTF due to the incident solar radiation can be evaluated. To do this, the divergence of q_r is inserted into the energy transport equation as a volumetric heat source term. This is a valid approximation to make as the radiative energy of the system is in equilibrium with the other modes of energy transport [10]. Therefore, the energy transport equation can be written as

$$\bar{C}_p(x)u(x,y)\frac{\partial T(x,y)}{\partial x} = \bar{k}(x)\frac{\partial T^2(x,y)}{\partial y^2} - \frac{\partial q_r(x,y)}{\partial y} \tag{10}$$

where $u(x,y)$ is the velocity profile in the fluid, $\bar{C}_p(x) = \frac{1}{L_y}\int_{y=0}^{y=L_y} C_p(x,y)dy$ is the mean volumetric heat capacity of the HTF at a given x-position, and $\bar{k}(x) = \frac{1}{L_y}\int_{y=0}^{y=L_y} k(x,y)dy$ is the mean thermal conductivity of the HTF at a given x-position. The boundary conditions associated with Equation 13 are

$$T(x=0,y) = T_{in}, \tag{11}$$

$$0 = -\bar{k}(x)\frac{\partial T(x,y=0)}{\partial y}, \tag{12}$$

$$0 = -\bar{k}(x)\frac{\partial T(x,y=L_y)}{\partial y}. \tag{13}$$

Since the receiver tube is encased by a vacuum the system does not lose thermal energy due convection. Therefore, from a convection and conduction perspective the boundary conditions are adiabatic. A thermal re-emission term is not included in Equation 12 because thermal re-emission from the HTD is accounted for by solving the RTE over the entire spectrum. A thermal re-emission term is commonly included in the boundary condition described in Equation 12 that is based on the surface temperature of the HTF [1]. This is not a valid assumption under all nanofluid conditions because thermal re-emission from a fluid is a volumetric process and not a surface phenomenon. Therefore, solving for the radiation intensities via the RTE over both the entire spectrum (including the solar and infrared spectrums) allows for a more accurate and computationally simpler determination of the heat flux and temperature in the HTF.

To calculate the temperature profiles based on the governing Equations 10 through 13, we followed an iterative method outlined by Kumar and Tien [10] that couples the RTE and the energy transport equation. Initially, the inlet temperature profile is the only known quantity. Using the inlet temperature of the HTF, the RTE can be solved to determine $q_r(y)$ and $\frac{\partial q_r(x,y)}{\partial y}$ at the $x = 0$ position The temperature profile along the y-axis at each subsequent x-position is then computed by solving Equations 10 through 13. To do this, the finite difference method was employed. Equations 14, 15, and 16 demonstrate the finite difference method used [10]

$$\begin{aligned}&\left(\frac{1}{2}\overline{C}_p u(y=0)+\frac{\Delta x}{\Delta y^2}\overline{k}\right)T(x_{i+1},y_0)-\frac{\Delta x}{\Delta y^2}\overline{k}T(x_{i+1},y_1)\\&=\frac{1}{2}\overline{C}_p u(y=0)T(x_i,y_0)-\frac{\Delta x}{2}\frac{\partial q_r(x_{i+1},y_0)}{\partial y},y_0=0\end{aligned}, \tag{14}$$

$$\begin{aligned}&\left(\overline{C}_p u(y_j)+\frac{2\Delta x}{\Delta y^2}\overline{k}\right)T(x_{i+1},y_j)-\frac{\Delta x}{\Delta y^2}\overline{k}\left(T(x_{i+1},y_{j+1})+T(x_{i+1},y_{j-1})\right)\\&=\overline{C}_p u(y_j)T(x_i,y_j)-\Delta x\frac{\partial q_r(x_{i+1},y_j)}{\partial y},0<y_j<L_y\end{aligned}, \tag{15}$$

$$\frac{\Delta x}{\Delta y^2}\overline{k}\left(T(x_{i+1},y_{L_y})-T(x_{i+1},y_{L_y-1})\right)=\frac{\Delta x}{\Delta y}q_r(x_{i+1},y_{L_y})-\frac{\Delta x}{2}\frac{\partial q_r(x_{i+1},y_{L_y})}{\partial y},y_{L_y}=L_y. \tag{16}$$

Previous studies that have utilized the RTE and energy equations to analyze the radiation through nanofluids have assumed laminar flow to be present [4, 10]. Laminar flow conditions are rarely present in CSP and other solar-to-thermal energy conversion technologies. For example, the Reynold's number (Re) for Therminol VP-1 at a temperature of 566 K traveling through a 76 mm diameter tube with a mass flow rate of 12 kg/s is Re = 675082 (density = 825 kg/m^3, u = 2.5 m/s, viscosity = 0.000234 Pa-s) [21]. Since PTC receivers are commonly in a turbulent flow regime we

add a turbulent component to the effective thermal conductivity of the HTF, where $\bar{k}(x) = \bar{k}_{Therminol}(x) + \bar{k}_{turb}(x)$. Here, $\bar{k}_{Therminol}$ is the mean thermal conductivity of the Therminol VP-1 and $\bar{k}_{turb}$ is the mean thermal conductivity due to mixing in turbulent flow conditions. To approximate turbulent flow conditions we assume that the velocity profile follows a 7th order power law velocity profile, where $u(x,y) = u_{\max}(x)\left(1 - \frac{\left|L_y/2 - y\right|}{L_y/2}\right)^{\frac{1}{7}}$. The parameter $u_{\max}$ is the maximum velocity at a given x-position and is determined by matching $\dot{m} = \int_{y=0}^{y=L_y} u(x,y)\rho(x)L_y\,dy$ = 12 kg/s, where ρ is the mean density of the Therminol VP-1 at each x-position. While k_{turb} is expected to be dependent on the y-position, a single value of k_{turb} is required at each x-position to solve Equations 10-13. Therefore, we determine $\bar{k}_{turb}$ using the relationship $\bar{k}_{turb}(x) = \frac{1}{L_y}\int_{y=0}^{y=L_y} k_{turb}(x,y)dy$. Numerous methods can be utilized to determine $k_{\text{turb}}(x,y)$ as a function of y-position, but the Prandtl mixing-length theory was employed in this study. [22] provides a thorough analysis of momentum and heat transfer mixing in turbulent boundary layers. It was found that after 3 iterations at each point in x-direction, the temperature in y-axis converges to within 1% of the final value which is obtained by calculating the temperature for by iterating more than ten times.

After the temperature profiles and radiative heat fluxes have been calculated across the tube's x and y dimensions, the solar-to-thermal effieciency of the system, η, can be equated. Here, η is defined as the ratio between the energy absorbed into the fluid and the incident solar radiation,

$$\eta = \frac{\int_{x=0}^{x=L_x} \dot{m}\bar{C}_p \, d\bar{T}}{q_{inc}}, \tag{17}$$

where $\bar{T}(x) = \frac{1}{L_y}\int_{y=0}^{y=L_y} T(x,y)dy$ is the mean temperature of the HTF across the *y*-axis.

3. Temperature distributions

Figure 3 shows temperature profiles within the solar receiver for Therminol VP-1 HTF seeded with Ag nanoparticles at a volume fraction of f_v = 9.5 × 10^{-5}. The receiver tube has a diameter, L_y = 76 mm, the inlet temperature is T_{in} = 566 K, the mass flow rate of the Therminol VP-1 is 12 kg/s, and the incident solar heat flux is q_{inc} = 40 suns (1 sun = 1000 W/m^2). Figure 3(a) shows the temperature of the HTF as a function of the HTF depth (along the *y*-axis) at various locations along the solar receiver (*x* = 0 m is the inlet and *x* = 920 m is the outlet). Since the HTF is in a turbulent flow regime, the effective thermal conductivity of the HTF due to mixing is high, resulting in a small variation in the temperature as a function of HTF depth. Figure 3(b) shows $\bar{k}_{turb}$ as a function of *x*-position along the receiver, which has a large value of thermal conductivity compared to the intrinsic thermal conductivity of the HTF itself. Finally, the mean temperature along the receiver is shown in Figure 3(c).

The thermal properties of Therminol VP-1 are based on the following equations [21]

$$\begin{aligned} k_{Therminol} &= -8.19477\times10^{-5}T - 1.92257\times10^{-7}T^2 \\ &+2.5034\times10^{-11}T^3 - 7.2974\times10^{-15}T^4 + 0.137743 \end{aligned}, \tag{18}$$

$$c_{Therminol} = 2.414T + 5.9591\times10^{-3}T^2 - 2.9879\times10^{-5}T^3 + 4.4172\times10^{-8}T^4 + 1498 \tag{19}$$

$$\rho_{Therminol} = -0.90797T + 0.00078116T^2 - 2.367\times10^{-6}T^3 + 1083.25, \tag{20}$$

where T is the temperature of Therminol VP-1 in Celsius, $c_{\text{Therminol}}$ is Therminol VP-1's specific heat in units of J/kg-K, and $\rho_{\text{Therminol}}$ is Therminol VP-1's density in units of kg/m^3.

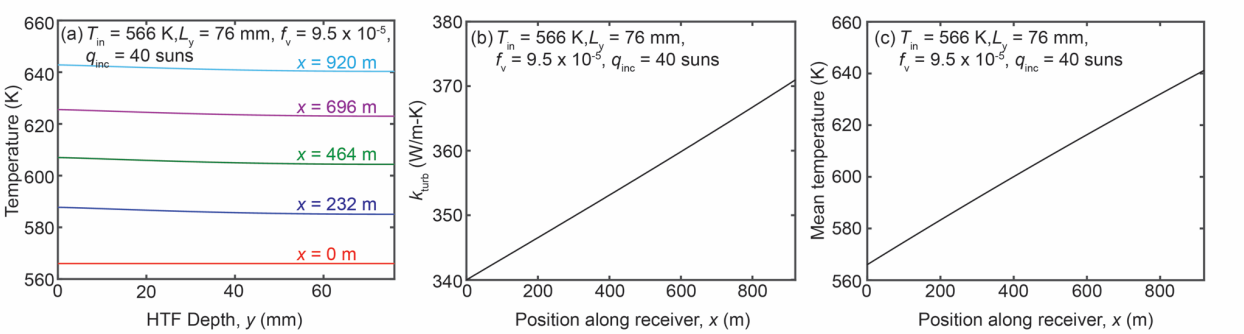

Figure 3: Temperature and thermal conductivity profiles for Therminol VP-1 seeded with Ag nanoparticles and $f_v = 9.5 \times 10^{-5}$. The receiver tube has a diameter, L_y = 76 mm, the inlet temperature is T_{in} = 566 K, the mass flow rate of the Therminol VP-1 is 12 kg/s, and the incident solar heat flux is 40 suns. (a) Temperature profiles of the HTF as a function of depth along the y-axis at various positions along the receiver tube. (b) The effective thermal conductivity due to mixing during turbulent flow conditions, k_{turb}, as a function of position along the receiver. Due to the high values of k_{turb} the temperature profiles in (a) exhibit small temperature variations along the y-axis. (c) The mean/bulk temperature of the HTF as a function of position along the receiver tube.

4. Solar-to-thermal conversion optimization

Using the model detailed in the previous section we now present an examination of η optimization by controlling the nanoparticle f_v in the nanofluid. Figure 4(a) shows η as a function of f_v for a solar receiver with Therminol VP-1 seeded with Ag nanoparticles as the HTF. The

incident solar heat flux ranges from 10 to 40 suns, which is consistent with solar heat flux values in PTC CSP plants. It should be noted that because $n_{\text{Therminol}} = 1.65$, the maximum η possible is ~89%. This is because ~11% of the incident radiation is reflected at the vacuum-Therminol VP-1 interface, based on Snell's law. To increase the maximum value of η that is theoretically possible, anti-reflection coatings or other devices that capture and harness the reflected radiation can be developed. As f_v increases from 10^{-8} to ~10^{-4}, η increases and reaches a maximum. The values of η then decrease with increasing f_v. The maximization of η can be explained by an examination of Figure 4(c), which plots the spectral radiative heat flux at the $x = 0$ and $y = 0$ coordinates of the solar receiver, based on the RTE. Increasing f_v enhances the absorption of the incident solar radiation (wavelengths between ~200 nm and ~2.5 μm). Therefore, the greater the value of f_v, the greater the absorbed solar heat flux at the surface. A positive heat flux here indicates radiation travelling into the fluid, whereas a negative heat flux indicates radiation travelling in a direction outwards and into the ambient environment. As f_v continues to increase, the emissivity of the nanofluid increases and the energy lost due to thermal re-emission increases. This can be seen in the infrared spectrum (~3 μm to ~30 μm), where the negative heat flux increases with increasing f_v. Therefore, an optimal f_v exists that produces both a high absorptivity over the solar spectrum and a low emissivity in the infrared spectrum for the nanofluid. The optimal f_v and η increase as q_{inc} increases because the incident solar radiation begins to outweigh the losses due to re-emitted thermal radiation, which eventually become negligible compared to the incident radiation.

Figure 4(b) shows η as a function of f_v under similar conditions as Figure 4(a), but $T_{\text{in}} = 300$ K. Since the temperature of the nanofluid is comparable to the temperature of the ambient environment, the losses due to re-emitted thermal radiation are negligible, as shown in Figure 4(d) (small negative heat flux in the infrared spectrum). Therefore, increasing the absorptivity of the

nanofluid in the solar spectrum is the principle method to increase and optimize η. The inset in Figure 4(b) demonstrates that an optimal f_v exists even at low nanofluid temperatures because the re-emitted heat flux becomes large enough to lower η at $f_v >> 10^{-4}$.

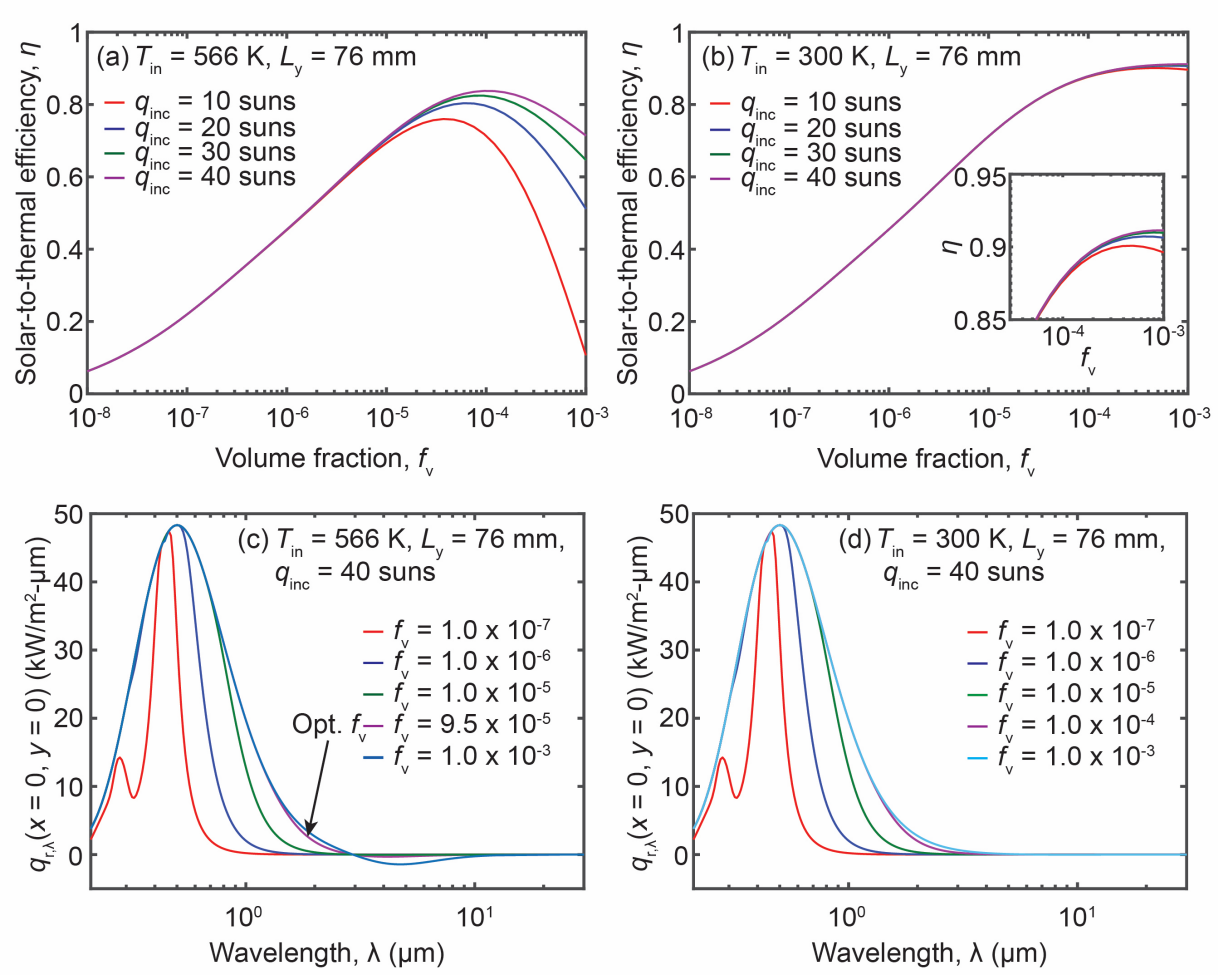

Figure 4: (a and b) Solar-to-thermal conversion efficiency as a function of f_v for four different incident solar concentrations with Ag nanoparticle-seeded Therminol VP-1 in a tube with a receiver depth of L_y = 76 mm and (a) T_{in} = 566 K / (b) T_{in} = 300 K. (c and d) Spectral radiative heat flux at the surface of the receiver tube, x = y = 0, for an array of f_v values. A positive heat flux indicates that heat is absorbed by the receiver, while a negative heat flux represents re-emitted thermal radiation

losses. The thermal radiation losses are greater in (c) than (d) because the temperature of the HTF is far greater.

While f_v is a convenient metric to determine the concentration of nanoparticles seeded within the nanofluid, the optimal f_v is dependent upon the value of L_y. Therefore, optical thickness, τ, can be a more useful metric to measure the quantity of nanoparticles seeded within the nanofluid because τ is independent of the receiver's thickness, L_y. Optical thickness is based on the extinction decay length on a spectral and direction basis. Since we have solved the RTE on a spectral and directional basis, τ is defined as an average over the directional and spectral incident solar radiation,

$$\tau = -\ln\left[\frac{\int_0^{\lambda}\int_0^{\pi/2} e^{-\frac{\sigma L_y}{\mu}} A\left(1-\rho_0\left(+\mu\right)\right) I_{bb,\lambda}\left(T_{sun}\right)\cos\theta d\theta d\lambda}{q_{inc}}\right]. \tag{21}$$

Figure 5(a) shows η as a function of f_v for five different values of L_y with q_{inc} = 40 suns and T_{in} = 566 K. Figure 5(b) shows the same four curves from Figure 5(a), but plotted as a function of τ. For small values of f_v all the curves in Figure 5(a) collapse to the same curve in Figure 5(b) when plotted as a function of τ. Therefore, the efficiency of the system is independent of L_y for small values of τ. As τ increases the solar-to-thermal efficiency of the system is dependent upon the receiver depth. This is because the temperature of the HTF increases with greater L_y causing thermal re-emission to become a significant thermal loss.

Industrial PTC systems normally vary the mass flow rate of the HTF to achieve a desired HTF temperature at the outlet of the tube. In this study we have instead set a constant mass flow rate to simplify our analysis. To facilitate further understanding of the relationship between temperature and efficiency in our system, Table 1 provides the mean outlet temperature, T_{out}, of the HTF for the conditions shown in Figure 5(b) with $\tau = 3$. Even though T_{out} increases as L_y increases, η decreases. This is because at the elevated temperatures in this analysis the energy losses due to thermal re-emission increase rapidly as the temperature of the HTF increases.

L_y (mm)	T_{out} (K)	η
76	641	0.83
152	690	0.66
380	789	0.52
608	829	0.40
760	841	0.35

Table 1: Outlet temperatures, T_{out}, for each receiver diameter condition shown in Figure 5(b) with $\tau = 3$.

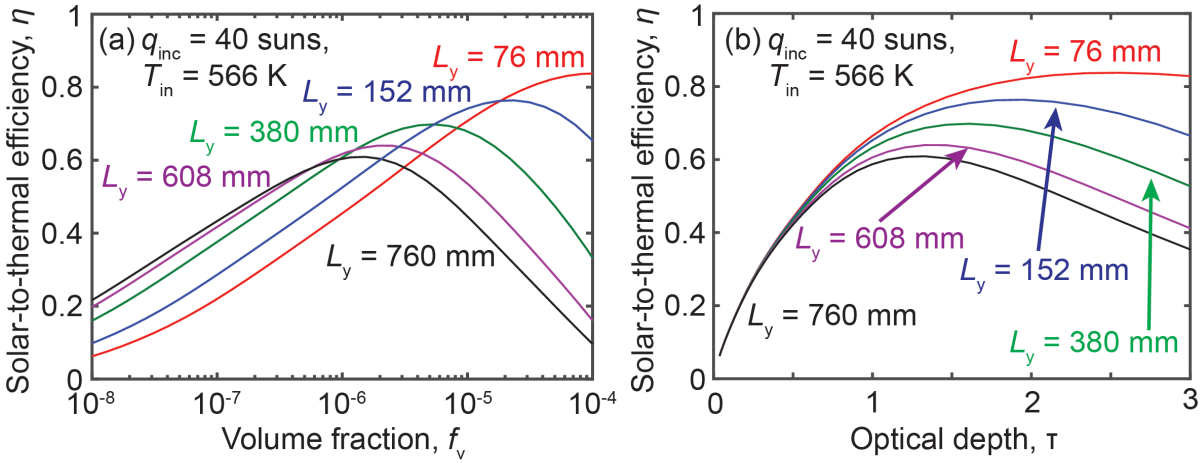

Figure 5: (a) Solar-to-thermal conversion efficiency as a function of f_v for five different receiver depths. (b) Solar-to-thermal conversion efficiency as a function of τ for five different receiver depths. For small values of optical depth all four curves from (a) collapse to one curve that is independent of L_y.

5. Effect of tube diameter

Current industrial parabolic trough configurations that employ selective solar absorbers (surface heating) use tube diameters that are 10s of millimeters in diameter. This receiver tube size enables reasonably high η, but requires a large pressure drop (ΔP) to pump the HTF. Increasing the receiver tube diameter can dramatically lower the pressure drop associated with pumping the HTF. Unfortunately, for surface-based heating tubes an increased tube diameter decreases η. A distinct advantage of direct solar volumetric absorption receivers is that the optimal efficiency (τ-dependent) of the receiver remains high even as the tube diameter increases.

Figure 6 shows the effects of tube diameter on η and ΔP for surface-based receiving tubes and nanofluid-based volumetric absorbing receiving tubes (Ag nanoparticles seeded in Therminol VP-1). On the left y-axis (blue), η normalized by the value of η_D = 76 mm (the solar-to-thermal efficiency of the system when the tube diameter is 76 mm) is plotted. The τ-dependent optimal solar-to-thermal efficiency (η_{Opt}) for volumetric heating is plotted in solid blue as a function of tube diameter and the surface-based η is plotted with a dashed blue line. For the surface-based receiver we assumed that the absorptivity of the selective solar absorber coating was 0.963 across all temperatures, the emissivity of the coating was 0.1 across all temperatures, and the HTF was Therminol VP-1 (no nanoparticle seeding). An incident solar concentration of 40 suns was used

with an inlet temperature of 566 K and a mass flow rate of 12 kg/s for both the surface-based and volumetric receivers. The heat transfer coefficient of the surface-based receiver (h), $h = k_{Therminol} Nu / L_y$, was determined based on the Nusselt number (Nu) under turbulent flow conditions, $Nu = 0.0256\,\mathrm{Re}^{0.79}\,\mathrm{Pr}^{0.42}$, where Pr is the Prandtl number. The thermal conductivity, density, and specific heat of Therminol VP-1 were determined based on Equations 18-20 and the dynamic viscosity of Therminol VP-1 in units of Pa-s was based on [21]

$$\mu_{Therminol} = \frac{\rho_{Therminol}}{10^6} \exp\left[\frac{544.149}{T + 114.43} - 2.59578\right], \tag{22}$$

where T is temperature in Celsius and $\rho_{Therminol}$ is in units of kg/m^3. The value of η for surface based receiver decreases by ~50% when the tube diameter is 625 mm compared to a tube diameter of 76 mm, while the efficiency of the volumetric absorber only reduces by ~20%.

The right y-axis (red) of Figure 6 shows ΔP normalized by the values of ΔP_D = 76 mm (the pressure drop when the tube diameter is 76 mm). The value of ΔP was calculated using empirical relations for the friction factor under turbulent conditions [22]

$$\Delta P = \int_{x=0}^{x=L_x} \frac{0.184\,\mathrm{Re}^{-0.2}\,\rho_{Therminol} u_m^2}{2L_y} dx, \tag{23}$$

where u_m is the mean velocity of the HTF in the tubes. The value of ΔP is roughly the same for both the surface and volumetric receivers and decreases dramatically by roughly four orders of magnitude as the hydraulic tube diameter increases by a factor of ~8 for both the surface-based receiver and the direct volumetric absorption receiver. Therefore, a direct volumetric absorption

receiver has the unique advantage of high η across all tube diameters coupled with an extremely small pressure drop that is necessary to pump the HTF at large tube diameters.

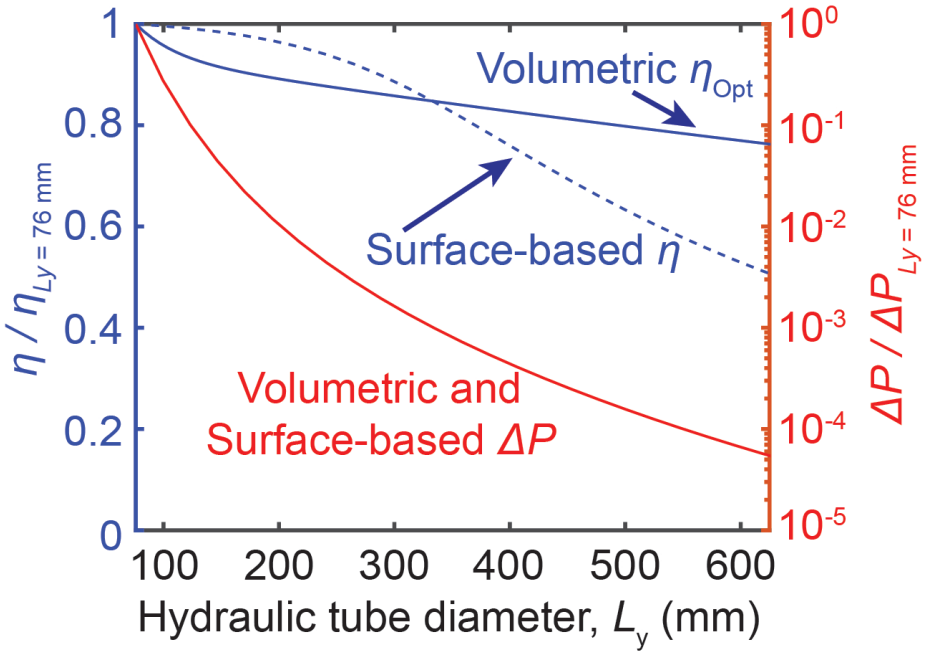

Figure 6: (Left *y*-axis) Normalized solar-to-thermal efficiency for volumetric and surface-based receivers. (Right *y*-axis) Normalized pressure drop required to pump the HTF.

6. Conclusion

In this study we presented a theoretical framework that for the first time accurately evaluates and optimizes η at any receiver size, inlet temperature of the HTF, and incident solar heat flux. The coupled RTE and energy equations accurately account for re-emitted thermal radiation losses by solving the RTE over the solar and infrared spectrums without making any assumptions in the infrared spectrum. Our analysis shows that the optimization of η is dependent

on the incident radiation and the volumetric fraction/optical depth of the nanofluid. Furthermore, we demonstrated that a direct volumetric absorption receiver is highly advantageous over a surface-based receiver because it has high η at large hydraulic tube diameters. This result enables large tube diameters to be used in a parabolic trough configuration while small values of ΔP are required to pump the HTF.

[1] Lenert, A., and Wang, E. N., 2012, "Optimization of nanofluid volumetric receivers for solar thermal energy conversion," Sol Energy, 86(1), pp. 253-265.
[2] Bermel, P., Lee, J., Joannopoulos, J. D., Celanovic, I., and Soljacie, M., 2012, "Selective solar absorbers," Begell house, Annual review of heat transfer, pp. 231-254.
[3] Otanicar, T. P., Phelan, P. E., Prasher, R. S., Rosengarten, G., and Taylor, R. A., 2010, "Nanofluid-based direct absorption solar collector," J Renew Sustain Ener, 2(3).
[4] Tyagi, H., Phelan, P., and Prasher, R., 2009, "Predicted Efficiency of a Low-Temperature Nanofluid-Based Direct Absorption Solar Collector," J Sol Energ Asme, 131(4).
[5] Taylor, R. A., Phelan, P. E., Otanicar, T. P., Adrian, R., and Prasher, R., 2011, "Nanofluid optical property characterization: towards efficient direct absorption solar collectors," Nanoscale Res Lett, 6.
[6] Bohn, M. S., and Wang, K. Y., 1988, "Experiments and Analysis on the Molten-Salt Direct Absorption Receiver Concept," J Sol Energ Asme, 110(1), pp. 45-51.
[7] Huang, B. J., Wung, T. Y., and Nieh, S., 1979, "Thermal-Analysis of Black Liquid Cylindrical Parabolic Collector," Sol Energy, 22(3), pp. 221-224.
[8] Minardi, J. E., and Chuang, H. N., 1975, "Performance of a Black Liquid Flat-Plate Solar Collector," Sol Energy, 17(3), pp. 179-183.
[9] Gupta, H. K., Das Agrawal, G., and Mathur, J., 2015, "An experimental investigation of a low temperature Al2O3-H2O nanofluid based direct absorption solar collector," Sol Energy, 118, pp. 390-396.
[10] Kumar, S., and Tien, C. L., 1990, "Analysis of Combined Radiation and Convection in a Particulate-Laden Liquid-Film," J Sol Energ Asme, 112(4), pp. 293-300.
[11] Kumar, S., Majumdar, A., and Tien, C. L., 1990, "The Differential-Discrete-Ordinate Method for Solutions of the Equation of Radiative-Transfer," J Heat Trans Asme, 112(2), pp. 424-429.
[12] Fernandez-Garcia, A., Zarza, E., Valenzuela, L., and Perez, M., 2010, "Parabolic-trough solar collectors and their applications," Renew Sust Energ Rev, 14(7), pp. 1695-1721.
[13] Blair, N., Dobos, A. P., Freeman, J., Neises, T., Wagner, M., Ferguson, T., Gilman, P., and Janzou, S., 2014, "System advisor model, SAM 2014.1.14: General description," National Renewable Energy Laboratory.
[14] Otanicar, T. P., Phelan, P. E., and Golden, J. S., 2009, "Optical properties of liquids for direct absorption solar thermal energy systems," Sol Energy, 83(7), pp. 969-977.

[15] Lupfert, E., Pottler, K., Ulmer, S., Riffelmann, K-J., Neumann, A., Schiricke, B., 2006, "Parabolic trough optical performance analysis techniques," J Sol Energy Eng, 129(2), pp. 147-152.
[16] Schiricke, B., Pitz-Paal, R., Lupfert, E., Pottler, K., Pfander, M., Riffelmann, K-J., Neumann, A., 2009, "Experimental verification of optical modeling of parabolic trough collectors by flux measurement," J Sol Energy Eng, 131(1), pp. 011004.
[17] Rakic, A. D., Djurisic, A. B., Elazar, J. M., Majewski, M. L., 1998, "Optical properties of metallic films for vertical-cavity optoelectronic devices," Applied Optics, 37(22), pp. 5271-5283.
[18] Hagemann, H. J., Gudat, W., and Kunz, C., 1975, "Optical-Constants from Far Infrared to X-Ray Region - Mg, Al, Cu, Ag, Au, Bi, C, and Al2o3," J Opt Soc Am, 65(6), pp. 742-744.
[19] Kerker, M., 1969, The scattering of light, and other electromagnetic radiation, Academic Press, New York.
[20] Bohren, C. F., and Huffman, D. R., 1983, Absorption and scattering of light by small particles, Wiley, New York.
[21] Solutia, "Therminol VP-1 vapor phase, liquid phase heat transfer fluid 12C to 400C," http://twt.mpei.ac.ru/tthb/hedh/htf-vp1.pdf.
[22] Incropera, F. P., DeWitt, D. P., and Incropera, F. P., 1985, Fundamentals of heat and mass transfer, Wiley, New York.